ORIGINAL PAPER

Influence of Relative Pile-Soil Stiffness and Load Eccentricity on Single Pile Response in Sand Under Lateral Cyclic Loading

Sudip Basack · Sandip Dey

Abstract The environment prevalent in ocean necessitates the piles supporting offshore structures to be designed against lateral cyclic loading initiated by wave action, which induces deterioration in the strength and stiffness of the pile-soil system introducing progressive reduction in the bearing capacity associated with increased settlement of the pile foundation. A thorough and detailed review of literature indicates that significant works have already been carried out in the relevant field of investigation. It is a well established phenomenon that the variation of relative pile-soil stiffness (K_{rs}) and load eccentricity (e/D) significantly affect the response of piles subjected to lateral static load. However, the influence of lateral cyclic load on axial response of single pile in sand, more specifically the effect of K_{rs} and e/D on the cyclic behavior, is yet to be investigated. The present work has aimed to bridge up this gap. To carry out numerical analysis (boundary element method), the conventional elastic approach has been used as a guideline with relevant modifications. The model developed has been validated by comparing with available experimental (laboratory model and field tests) results, which indicate the accuracy of the solutions formulated. Thereafter, the methodology is applied successfully to selected parametric studies for understanding the magnitude and pattern of degradation of axial pile capacity induced due to lateral cyclic loading, as well as the influence of K_{rs} and e/D on such degradation.

Abbreviations

A	Normalized amplitude of lateral cyclic loading
$\{b\}$	Augment vector for initial elastic analysis
$[C]$	Square matrix for initial elastic analysis
C_f	Static pile capacity factor
D	External pile diameter
D_f	Degradation function
D_p	Degradation factor for axial pile capacity
D_{si}	Soil degradation factor for ith node
e	Load eccentricity
E_p	Young's modulus of pile material
E_s	Young's modulus of soil
E_{si}	Young's modulus of soil at ith node
η_e	Rate of increase of Young's modulus of soil with depth
F_D	Coefficient for soil degradation parameter based on soil density
F_L	Coefficient for soil degradation parameter based on cyclic loading pattern

S. Basack (✉)
Department of Applied Mechanics, Bengal Engineering and Science University, Howrah 711103, India
e-mail: basackdrs@hotmail.com

S. Dey (✉)
Department of Civil Engineering, Bengal Engineering and Science University, Howrah 711103, India

F_I	Coefficient for soil degradation parameter based on pile installation
$[F_p]$	Finite difference coefficient matrix
γ'	Submerged unit weight of soil
γ_s	Bulk unit weight of soil
H	Lateral load applied on pile head
H_{max}	Maximum value of lateral cyclic load applied on pile head
H_{min}	Minimum value of lateral cyclic load applied on pile head
H_{us}	Static lateral pile capacity
I_p	Moment of inertia of pile cross section
$[I_s]$	Soil displacement influence factors matrix
i, j	Nodal point indicator
K_p	Passive earth pressure coefficient of soil
K_{rs}	Relative pile-soil stiffness
L	Embedded pile length
M_h	External moment applied at free pile head
M_i	Bending moment at *ith* node
M_y	Yield bending moment of pile
μ_s	Poisson's ratio of soil
n	Number of divisions
N	Number of cycles
$\{p\}$	Column matrix for elemental soil pressure
p_i	Elemental soil pressure
p_{ui}	Ultimate elemental soil pressure
P_{ac}	Cyclic axial pile capacity
P_{as}	Static axial pile capacity
ρ_h	Pile head deflection
ρ_i	Nodal displacements
$\{\rho\}$	Column matrix for nodal deflection
$\{\rho_p\}$	Column matrix for nodal deflection of pile
$\{\rho_s\}$	Column matrix for nodal deflection of soil
t	Soil degradation parameter
V_i	Nodal shear force
z	Depth below ground surface

1 Introduction

Offshore structures, namely, oil and gas exploration rigs, offshore helideck, tension leg platforms, jetties, etc. are mostly supported on pile foundations. Apart from the usual superstructure loads (dead load, live load, etc.), these piles are subjected to continuous cyclic loading (along axial or lateral direction or a combination) resulting from the wave action (Basack 2008a, b). It is a well established phenomenon that

such transient loading induces progressive deterioration on the pile-soil interactive performance resulting in gradual reduction in the pile capacity with increased displacement (Poulos 1981, 1982; Bea and Aurora 1982). The primary reason that may be assumed for such deterioration is the gradual occurrence of rearrangement and realignment of soil particles in the vicinity of the interface, although the development of excess pore water pressure and progressively developed irrecoverable plastic strain in the adjacent soil can as well be expected to contribute significantly to such degradation, specifically for clay (according to Prof. H. G. Poulos in a private communication, 2010). The pile response due to wave loading has been found to be governed by the cyclic loading parameters, viz., number of cycles, frequency and amplitude (Basack 1999). The design of offshore piles must satisfy the following criteria: adequate factor of safety against failure, acceptable displacements and constructional feasibility (Poulos 1988).

An extensive literature survey indicates that several approaches were suggested by various researchers to analyze the response of piles under lateral cyclic loading. Commencing from the empirical approaches (Gudehus and Hettler 1981), modified p–y curves method (Reese 1977; Allotey and El Naggar 2008) to more recent boundary element analysis (Poulos 1982; Basack 2008a, 2010b) and strain wedge model (Ashour and Norris 1999), the subject has undergone advancement. Although the relevant data on the degradation for piles in clay are available, the information in case of sand is rather limited.

It is observed that the lateral cyclic loading significantly affects the axial performance of piles (Narasimha Rao and Prasad 1993), although the available theoretical analyses covering this aspect in details are rather limited (Basack 2008a). Also, it is a well established phenomenon that the relative pile-soil stiffness (K_{rs}) and non-dimensional load eccentricity (e/D) produce remarkable influence on the behavior of laterally loaded pile (Broms 1964a, b), but the same is yet to be investigated on the performance of pile subjected to lateral cyclic loading.

The work reported herein is aimed towards carrying out numerical analysis based on boundary element method to study the influence of lateral cyclic loading on axial performance of single, vertical pile in sand and simultaneously the effect of the variation of K_{rs} and e/D.

2 Numerical Analysis

To investigate the effects of lateral cyclic loading on axial performance of *single, vertical, floating pile in sand*, a numerical model has been developed. Initially, analysis was conducted for pile subjected to static lateral load. Further extension was made to incorporate the effect of cyclic lateral loading. For computation, boundary element analysis was adopted. The methods proposed by Poulos (1971, 1982) were followed respectively as preliminary guidelines with necessary modifications in accordance with the relevance of the present problem.

2.1 Assumptions

The following assumptions are made to carry out the analysis:

(i)   The subsoil is a homogeneous, isotropic, semi-infinite and elastic-perfectly plastic material. When elastic, it has a constant Young's modulus (E_s) and Poisson's ratio (μ_s) which remain unaffected by the presence of the pile.

(ii)   The material of the pile is as well homogenous, isotropic and elastic-perfectly plastic.

(iii) When subjected to lateral loading, static or cyclic, the pile behaves as an elastic beam, till the material yielding takes place.

(iv)   The pile base is free against translation and rotation.

(v)   Possible horizontal shear stresses between the soil and the sides of pile are ignored.

(vi)   The soil always remains in contact of the pile surface during static or cyclic loadings.

2.2 Pile Under Lateral Static Load

As mentioned earlier, the elastic analysis proposed by Poulos (1971) has been followed as a guideline. The pile was idealized as a thin vertical plate having its width, embedded length and flexural rigidity equal to the diameter D, depth of embedment L and flexural rigidity E_pI_p of the actual pile (Fig. 1). A Lateral static load H is applied at a height of e above the ground surface. For free headed pile, a clockwise moment M_h has been applied at the pile head in addition.

The embedded portion of the pile is longitudinally discretized into $n + 1$ number of elements, where n is
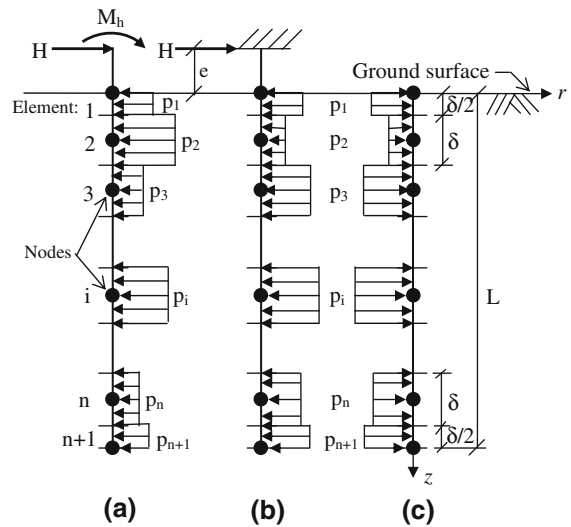
Fig. 1 The idealized problem for stresses acting on: **a** free headed pile. **b** Fixed headed pile. **c** Soil adjacent to pile surface

a positive integer greater than unity. Each of these elements is of equal length δ except the two extreme elements which are of length $\delta/2$. Analysis has been carried out for two extreme pile head conditions: free (i.e., no rotational restraint) and fixed (complete rotational restraint). In reality however, the pile head is expected to behave as partially fixed in most of the practical cases; but the same has not been considered in absence of adequate data. Under static load and moment, each of the *ith* pile elements is subjected to a lateral soil pressure p_i which is assumed to act uniformly over the surface of the entire element (Fig. 2). Initially, the focus is to evaluate the expressions for the displacements of the soil and the pile at the central nodal points of each of the elements and to apply a reasonable condition of displacement compatibility.

The soil displacements are obtained by integration of the equation given by Mindlin (1936) over each of the elements. The expressions already available from Douglas and Davis (1964) are utilized for this purpose. The soil displacement expressions have been written in matrix form as follows:

$$\{\rho_s\} = [I_s]\{p\} \tag{1}$$

where, the augment vectors $\{\rho_S\}$ and $\{p\}$ represent the relevant column matrices for the nodal soil displacements at the interface and the elemental soil pressures respectively and $[I_s]$ is a square matrix representing the
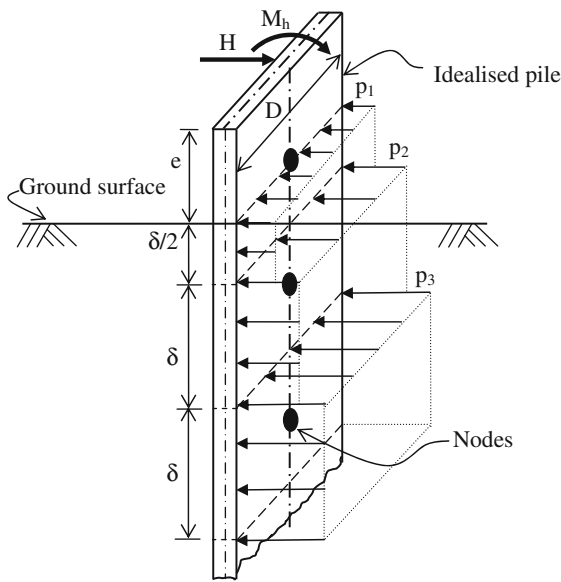
Fig. 2 3-D view of the discretized idealized pile

soil displacement influence factors as obtained by utilizing the expressions of Douglas and Davis (1964).

The nodal pile displacements, on the other hand, have been evaluated by expressing in finite difference form, the standard fourth order differential equation originating from the theory of bending an elastic beam [as per the assumption (iii) above]. For the two extreme elements, the bending equations are also used to eliminate the fictitious nodal displacements beyond the embedded pile length. The expressions in matrix form are as follows:

$$\{\rho_p\} = [F_p]\{p\} \tag{2}$$

where, $\{\rho_p\}$ is the vector for nodal pile displacements and $[F_p]$ is the finite difference coefficient matrix.

In order to form the matrix $[F_p]$, the 4th order differential equation for bending of the elastic pile (which is idealized as a thin beam) has been written in finite difference form for inner elements (i.e., $2 < i < n$). In case of the two extreme elements (i.e., $i = 1$ and $i = n + 1$), the 2nd order differential equation for bending of the elastic pile is used in addition as boundary conditions to eliminate the indeterminate nodal displacements.

From the assumption (vi) above, the condition of displacement compatibility holds good, i.e., the nodal displacements of the soil and those of the pile should be equal. Thus,

$$\{\rho_s\} = \{\rho_p\} = \{\rho\} \tag{3}$$

Eliminating the displacement matrices from Eqs. 1 and 2, and using two additional equations from the load and moment equilibrium conditions of the pile, the following matrix equation has been ultimately obtained:

$$[C]\{p\} = \{b\} \tag{4}$$

where, $[C]$ is a coefficient matrix of order $n + 1 \times n + 1$ and $\{b\}$ is the relevant augment vector.

The Eq. 4 above may be solved to obtain the initial values of the unknown soil pressure p_i, which are then compared with a specific yield pressure p_{ui} relevant to any *ith* element. If $|p_i| \geq |p_{ui}|$, the soil adjacent to the element is considered to have been yielded, i.e., that particular element has been assumed to have been *yielded*, and $|p_i|$ is replaced by $|p_{ui}|$. The soil pressures for the remaining elements are redistributed using the same Eq. 4 above, assuming the applicability of the Mindlin's equation for those elements where yielding has yet to occur (Poulos 1971). The procedure is recycled which may lead to progressive yielding of pile elements.

In the present analysis, the yield soil pressure p_{ui} at a certain depth for *sand* has been taken as three times the Rankine's passive earth pressure at that depth, after the recommendation of Broms (1964b). Although conservative, this value has been chosen in absence of any suitable correlation.

Accurate computation of the elemental soil pressures p_i is followed by evaluation of the nodal displacements ρ_i obtained from the pile displacement relations (Eq. 2 above). The expressions for pile head deflection ρ_h has been derived from the flexure equation of the pile above the ground surface and is written as follows:

$$\rho_h = \rho_1\left(1 + \frac{e}{\delta}\right) - \rho_2\frac{e}{\delta} + e\delta\frac{M_h + He}{2E_pI_p}$$
$$+ e^2\frac{3M_h + 2He}{6E_pI_p} \tag{5a}$$
(free headed pile)

$$\rho_h = \rho_1 + \frac{He^3}{3E_pI_p} + \frac{e^2\delta^2D}{2E_pI_p}\left(\frac{p_1 + p_{n+1}}{2} + \sum_{j=2}^{n}p_j\right)$$
(fixed headed pile) \hfill (5b)

As opposed to the free headed pile, a fixing moment is developed at the pile head in case of the fixed headed

pile, whose value is computed using the moment equilibrium condition of the portion of the pile below the ground surface. This is the reason for inclusion of the elemental soil pressures p_i in the expression for the pile head deflection of the fixed headed pile, although both the Eqs. 5a and 5b above are derived using the flexure equation of the portion of pile above the ground surface.

The nodal bending moments and shear forces produced in the pile are calculated by considering the equilibrium of the portion of pile below the ground surface (Basack 1999). Using the moment and load equilibrium conditions of the portion of pile between the base and the cross section corresponding to the nodal point under consideration, the bending moments and the shear forces are calculated at the nodes. Since the pile is a floating pile (see Sect. 2 above), the pile base is free to rotate and hence the bending moment is zero at the base. The resulting expressions for nodal bending moment and shear force developed in the pile are given by:

$$M_j = - \left[\frac{\delta D}{8} p_j + \frac{\delta D}{2} \left(L - (j-1)\delta - \frac{\delta}{4} \right) p_{n+1} \right.$$
$$\left. + \delta^2 D \sum_{k=j+1}^{n} (k-j) p_k \right] \qquad (6a)$$

$$V_j = D\delta \left(\frac{p_{n+1}}{4} + \frac{p_j}{2} + \sum_{k=j+1}^{n} p_k \right) \qquad (6b)$$

where, M_j and V_j are the bending moment and shear force developed in the pile at the *jth* nodal point respectively. The bending moment causing convex curvature of the elastic curve on the backward side of the pile has been chosen positive. Likewise, the shear force at any cross section causing a tendency of the upper portion of pile to move forward is considered positive.

In case of relatively flexible piles, the yielding of its material due to bending was found to take place prior to occurrence of the complete soil yield throughout the depth of embedment (Broms 1964a, b). This phenomenon has been incorporated while evaluating the lateral static pile capacity H_{us}, where the value of H is increased in small steps. The load corresponding to which the yielding of soil takes place for all the elements or the maximum nodal bending moment exceed the yield value for the pile under consideration,

whichever is less, is chosen as the lateral static capacity of the pile.

In the analysis, it is assumed that the soil always remains in contact with the pile surface during static and cyclic loadings [assumption (vi) above]. However, because of a limited ability of soil to take tension, a tension crack/cutoff is likely to be developed in the soil adjacent to the interface in the vicinity of the ground surface (Poulos and Davis 1980) inducing increase in the pile displacements (Douglas and Davis 1964), but in most practical cases, this increase is about 30–40% for relatively flexible pile ($K_{rs} < 10^{-5}$). Although investigation carried out by the author (Basack 2010a, b) indicated that the effect of this soil-pile separation is remarkable in cohesive soil, the same does not significantly affect the pile-soil response in cohesionless soil and hence not considered in the present analysis.

2.3 Pile Under Lateral Cyclic Load

The above analysis has been extended to take into account the effect of lateral cyclic loading. The approach of Poulos (1982) is used as a preliminary guideline with necessary additions. The cyclic response of the pile is governed by the following two significant phenomena:

(i) Progressive degradation of p_{ui} and E_s in the vicinity of the interface.
(ii) Shakedown effect induced by the gradual accumulation of irrecoverable plastic deformation developed in the soil at the interface.

The cyclic analysis in regards to the soil degradation may be carried out following two alternative approaches, viz. cycle-by-cycle analysis (Matlock et al. 1978) or composite analysis (Poulos 1982). In the former case, enormous computational effort is required, especially when the number of cycles is quite large. In the later case, the values of cyclic strength and stiffness of soil are adjusted after completion of all the load cycles. This is an approximate method although has been reported to yield quite promising results. The later approach being convenient is adopted in the present analysis.

The degradation of soil strength and stiffness has been quantified by a term soil degradation factor D_{si}, defined as the ratio of the cyclic to pre-cyclic values of nodal soil strength and stiffness. Based on full scale

pile tests and other additional case histories, Long and Vanneste (1994) proposed the following relations for piles in sand:

$$D_{si} = N^{-t} \tag{7a}$$

$$t = 0.17\, F_L F_I F_D \tag{7b}$$

where, N is the number of cycles, t is a degradation parameter and F_L, F_I and F_D are the non-dimensional coefficients based upon details of the cyclic load ratio, pile installation, and soil density, respectively. Based on 34 full scale cyclic pile test case studies, the suggested values for F_L, F_I and F_D for various field conditions were summarized and presented by Long and Vanneste (1994).

While calculating the cyclic capacity of piles, the effect of shakedown has been incorporated. The cyclic capacity of the pile is calculated considering no contribution on the frictional resistance at the interface where yielding of soil has taken place and degraded values of soil strength and stiffness for the remaining portion of the interface and also for the base of pile where no soil yield has occurred. The post-cyclic pile capacity is calculated following conventional static method which is available in any standard text book (e.g., Poulos and Davis 1980). The degradation factor for pile capacity has been defined as follows (Purkayastha and Dey 1991):

$$D_p = \frac{P_{ac}}{P_{as}} \tag{8}$$

where, D_p is the degradation factor for cyclic pile capacity while P_{ac} and P_{as} are the cyclic and static (i.e., pre-cyclic) capacities of the pile. Henceforth in this paper, the term 'degradation factor' will indicate the degradation factor for cyclic pile capacity.

The amplitude A of lateral cyclic loading applied on the pile head has been expressed as a fraction of the lateral static capacity of pile and may be calculated from the Eq. 9 below:

$$A = \frac{H_{max} - H_{min}}{2H_{us}} \tag{9}$$

where, H_{max} and H_{min} are the maximum and minimum values of the cyclic lateral loads applied on the pile head respectively and H_{us} is the static lateral pile capacity.

Due to cyclic degradation, the soil modulus no more remains constant with depth. In such case, the

soil displacement at the ith nodal point due to soil pressure imposed on the jth element is computed using the soil modulus corresponding to the ith element, and the values of the soil displacement influence factors (see Eq. 1) are adjusted accordingly.

2.4 Computational Algorithm

The cyclic analysis has been carried out step-by-step sequentially. The steps of computation in the present analysis are as follows:

(i)   Analysis under lateral static load is conducted using initial input parameters for soil, pile and load. The elemental lateral soil pressures, nodal displacements, shear force and bending moments and lateral static pile capacity are calculated.

(ii) With the given values of N and degradation parameters, the nodal soil degradation factors D_{si} are calculated and the new values of p_{ui} and E_{si} are evaluated for all i.

(iii) Using these degraded values of the soil strength and stiffness, analysis is again carried out following the step (i) above taking the cyclic amplitude as the input value of H and the depth of soil yield is found out.

(iv) With the degraded values of the soil strength and stiffness and considering the effect of soil yield, the cyclic lateral and axial pile capacities, displacements, shear force and bending moments are computed.

(v)   After the static and cyclic pile capacities are computed, the pile degradation factor D_p has been evaluated from the Eq. 8.

2.5 Development of Computer Software

The entire computation has been carried out using a user-friendly computer software LCS developed by the authors in Fortran-90 language, the flowchart of which is given in Fig. 3.

3 Validation

In order to verify the accuracy, the numerical model described above has been validated by comparisons with the available results of model and field tests.
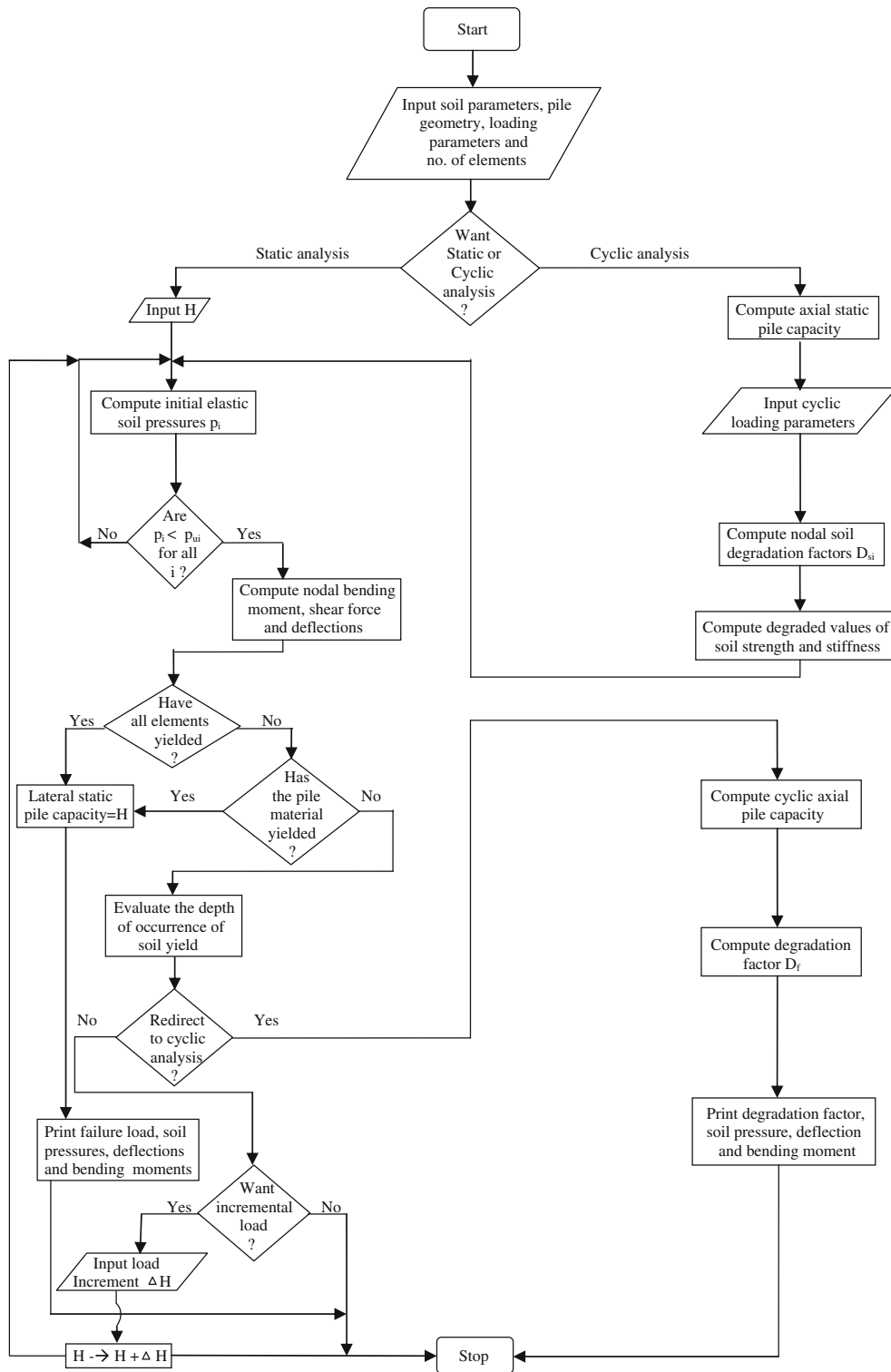
Fig. 3 Flowchart of the software LCS

Basack ([2008b]) carried out a series of small-scale laboratory model tests to study the effects of two-way lateral cyclic loading on a single pipe pile of steel (outer diameter 20 mm and wall thickness 5 mm) driven into a remoulded dense sand bed (relative density = 64%). The pile head was partially fixed, as evidenced from the loading mechanism. The inner surface of the pile was instrumented with 7 micro strain gauges, equally spaced, to observe the bending moment pattern. The soil bed was prepared in small layers, each being filled initially by rainfall technique and thereafter by compaction; as reported, the strength and stiffness of the remoulded test bed was observed to be fairly uniform with respect to depth. The model pile was driven into the prepared test bed by a screw-jack type of pile pushing equipment; the rate of pile installation was as low as 5 mm/min. The computational parameters adopted, obtained from Basack ([2008b]), are: $L = 500$ mm, $\gamma_s = 19$ kN/m^3, $\phi = 30°$, $e = 90$ mm, $E_p = 200$ GPa, $E_s = 78$ MPa (back-figured from the reported shear modulus value of 30 MPa obtained by direct shear test). The value of μ_s has been chosen as 0.3 (Poulos and Davis [1980]) and the soil degradation coefficients, chosen after the recommendations of Long and Vanneste ([1994]) for driven piles in dense sand under symmetric two way cyclic loading, are: $F_L = 0.2$, $F_I = 1.0$, and $F_D = 0.8$. The experimental pile bending moments, normalized by the yield moment of the pile ($M_y = 280$ Nm), corresponding to the cyclic amplitude of 0.2 are compared with those obtained by the present model (Fig. [4]). For adequate comparison, the computed bending moments are evaluated and plotted for both the free and the fixed pile head conditions. As observed, the basic nature of the theoretical curves is similar to the experimental one. In the range of $-0.2 \leq z/L \leq 0.4$, the experimental values are observed to lie in between the two curves. For $0.4 \leq z/L \leq 1.0$, on the other hand, the two theoretical curves almost coincide, whereas the experimental values are on the higher side, the average variation being about 25%. The computed bending moment was found to be maximum at depths of $z/L = 0.3$ and 0.4 for the free headed and fixed headed piles respectively as against the experimental value of about 0.35. The values of the computed maximum normalized bending moments are noted as 0.013 and 0.020 for the two pile head conditions respectively, against an experimentally obtained value of 0.018.
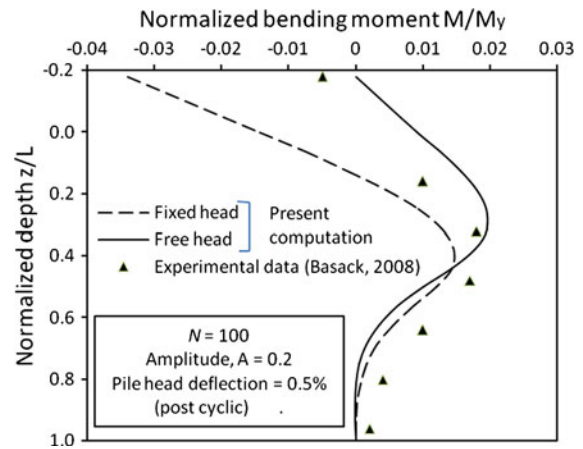
Fig. 4 Comparison of computed bending moments with the Model test results of Basack ([2008a], [b])

Taylor ([2006]) conducted full scale lateral cyclic load tests of a small diameter single pipe pile driven in sand. The pile conformed to ASTM 252 Grade 3 specifications having an outside diameter of 324 mm with a wall thickness of 9.5 mm and yield moment of 350 kNm. The depth of embedment was 13 m and the lateral load was applied at an eccentricity of 483 mm above the ground surface. The test represented free-head pile condition. The site was located 300 m on the north side of the Salt Lake International Airport, USA. The subsurface investigation carried out indicated the existence of layered soil, primarily sand and silt of various densities with few intermediate thin layers of silty clay; the groundwater table was located at a depth of 2 m below the surface. The pile was loaded to the target deflections of 6, 13, 19, 25, 38, 51, 64, 76, and 90 mm for a total of ten times in each case after which the load was released to allow for rebound. After completion of ten cycles for each target deflection, further ten cycles of loading were performed at the next higher deflection level. For the convenience of present computation, the average values of soil parameters taken are: $\gamma_s = 19$ kN/m^3, $\gamma' = 9$ kN/m^3, $\phi' = 39°$. From the average CPT value, the Young's modulus of the soil was estimated by the authors from the available correlations (Robertson and Campanella [1983]; Kulhawy and Mayne [1990]) as $E_s = 40$ MPa. The value of μ_s has been chosen as 0.3 (Poulos and Davis [1980]). The coefficients for cyclic degradation coefficients for driven pile in medium dense sand subjected to one-way lateral cyclic loading are chosen (after Long and Vanneste [1994]) as: $F_L = 1.0$,
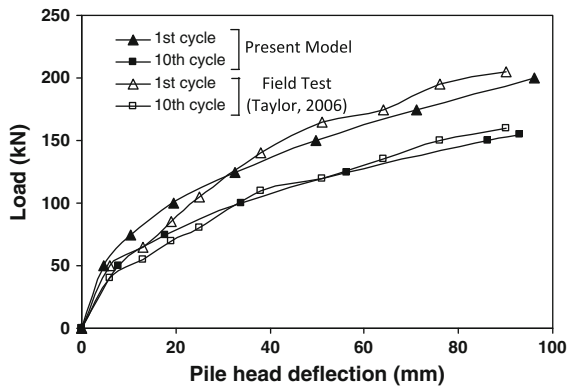
Fig. 5 Comparison of computed cyclic load–deflection prediction with the field test results of Taylor ([2006](#))

$F_I = 1.0$, and $F_D = 1.0$. The comparison of average peak load versus pile head deflection for the first and the tenth cycles are presented in Fig. 5. The computed curves are observed to be in reasonably good agreement with the field test results.

4 Parametric Studies

The response of a prototype concrete pile embedded in a medium dense sand bed under the action of symmetric two-way lateral cyclic loading has been studied in details. The soil parameters and pile geometry are shown in Fig. 6. The groundwater table was taken at the surface. The Young's modulus of soil was assumed to increase linearly with depth at a rate of $\eta_e = 5$ MPa (from the correlation of Terzaghi [1955](#)). Analysis has been carried out for both the free and the fixed pile head conditions. The yield stress of the pile material in bending is taken as 10 MPa. The
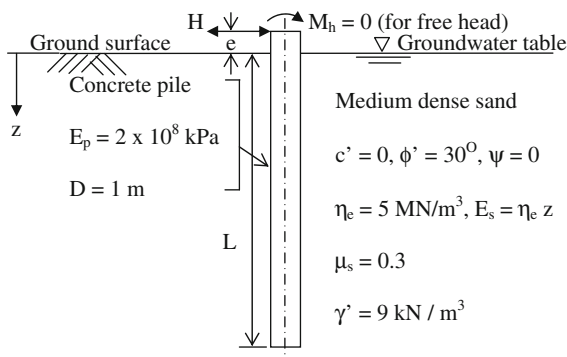
Fig. 6 The prototype pile considered for parametric studies

degradation coefficients adopted (after Long and Vanneste [1994](#)) are: $F_L = 0.2$, $F_I = 1.0$ and $F_D = 0.8$. Computations have been carried out by varying the depth of embedment from 10 to 35 m and the load eccentricity from 0 to 10 m. Following the recommendation of Poulos and Davis ([1980](#)), the relative pile soil stiffness for sand (K_{rs}) is obtained from the following relation:

$$K_{rs} = \frac{E_p I_p}{\eta_e L^5} \tag{10}$$

While conducting a sensitivity check by gradually increasing the number of elements, it is observed that its effect on the cyclic pile response is insignificant for $n > 100$ as compared to the computational effort required. Hence, analyses are carried out with $n = 100$.

4.1 Pile Response Under Lateral Static Load

The static lateral pile capacities for various L/D and e/D ratios and pile head conditions are computed following the procedure described earlier (Sect. 2.2, last paragraph) and running the computer software LCS. The static lateral pile capacities are found to be 20–30% lower compared to those of Broms ([1964b](#)) in case of free headed pile. Similar observation was also reported by Poulos and Davis ([1980](#)). As opposed to the analysis of Broms ([1964a](#)), the results obtained from the present computations are significantly affected by the pile flexural rigidity $E_p I_p$ and the Young's modulus of soil E_s, besides the L/D and e/D ratios. For fixed headed pile, on the other hand, the effect of load eccentricity (e) has been incorporated in addition as regards to present analysis; the same has not been considered by Broms ([1964b](#)).

The values of lateral static pile capacities, normalized by $K_p \gamma' D^3$, K_p being the passive earth pressure coefficient, are presented in Table 1. These nondimensionalised static lateral pile capacity are plotted against K_{rs} and e/D (Figs. 7, 8 respectively). The normalized static capacity is observed to vary in the range of 20–130 for free headed pile as against 40–280 in case of fixed head condition. Also, the capacity decreases quite sharply in a curvilinear manner for $K_{rs} \leq 10^{-3}$ and stabilizes thereafter. With increase in normalized load eccentricity, the pile capacity is found to decrease, the pattern of variation being curvilinear with decreasing slope. Specifically in the range of

$10 \leq L/D \leq 15$, a linear trend is observed for $e/D > 4$ beyond the initial curvilinear for the range of $0 \leq e/D \leq 4$. For identical parameters, the head fixity was observed to produce significant increase in static lateral pile capacity. The static capacity factor C_f, defined as the ratio of fixed headed to free headed lateral static pile capacities, are plotted against K_{rs} (Fig. 9). The values of C_f is found to vary from 1.67 to 2.4. As observed, C_f decreases quite sharply for initial values of $K_{rs} \leq 2.5 \times 10^{-4}$ with increasing slopes, attains minimum value and thereafter increases linearly.

4.2 Pile Response Under Lateral Cyclic Load

The pattern of variation of degradation factor with cyclic loading parameters and the effect of K_{rs} and e/D on the degradation factor are studied.

4.2.1 Cyclic Loading Parameters

As pointed by Basack (1999), the cyclic loading parameters are: number of cyclic, frequency and amplitude. For piles in sand however, the effect of the rate of loading is insignificant, although a slight rate effect of about 2–4% increase was observed in case of calcareous sand (Poulos 1988). Since the rate of loading does not significantly affect the pile-soil interactive performance in sand, the parameter 'frequency' is not considered in the present study. As mentioned earlier,
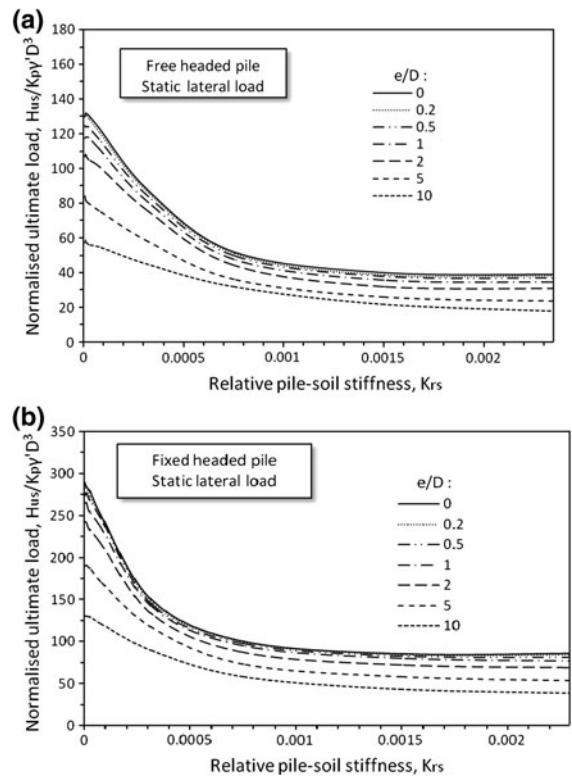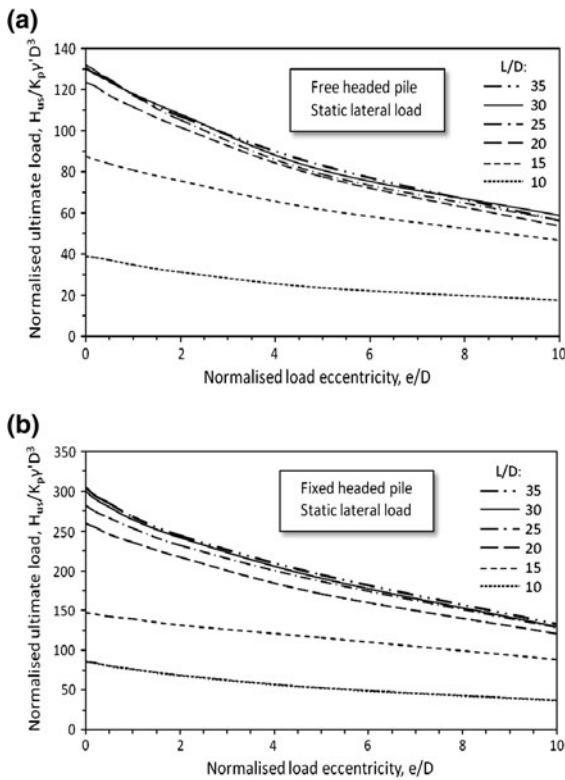
Fig. 7 Variation of normalized ultimate lateral static pile capacity with K_{rs} for pile head conditions: **a** free. **b** fixed

the amplitude of lateral cyclic loading applied on the pile head is expressed as a fraction of the corresponding lateral static pile capacity.

Table 1 Values of normalized static lateral pile capacity $H_{us}/(K_p\gamma'D^3)$

L/D	K_{rs}	e/D						
		0.0	0.2	0.5	1.0	2.0	5.0	10.0
10	2.45×10^{-3}	38.88[a]	38.52	37.04	34.81	31.11	23.7	17.4
		_85.55[b]_	_84.07_	_80.37_	_76.3_	_68.51_	_52.59_	_37.04_
15	3.23×10^{-4}	87.41	85.92	84.07	80.74	75.56	61.48	46.67
		_147.78_	_145.92_	_142.96_	_140_	_131.85_	_115.56_	_88.15_
20	7.66×10^{-5}	123.7	121.48	117.04	111.48	101.48	77.41	53.7
		_251.48_	_249.26_	_246.3_	_235.92_	_217.04_	_171.48_	_120.74_
25	2.51×10^{-5}	130.74	127.78	124.07	117.78	105.18	78.89	56.3
		_279.63_	_272.96_	_268.15_	_254.07_	_232.59_	_186.67_	_128.52_
30	1.01×10^{-5}	131.85	129.26	124.07	118.15	108.15	80.74	58.89
		_284.07_	_284.81_	_276.3_	_264.81_	_241.85_	_190.37_	_130_
35	4.67×10^{-6}	130	127.78	124.81	117.41	107.04	82.96	56.3
		_288.89_	_281.12_	_272.96_	_264.07_	_242.23_	_189.63_	_129.63_

[a] Normal font means free headed pile, [b] Italized font means fixed headed pile

Fig. 8 Variation of normalized ultimate lateral static pile capacity with *e/D* for pile head conditions: **a** free. **b** fixed
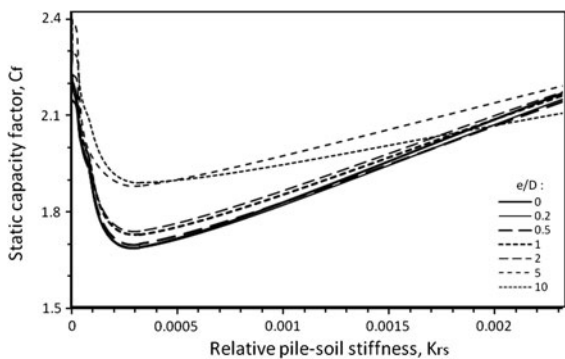
Fig. 9 Variation of C_f with K_{rs}

The plot of degradation factor D_p versus number of cycles and amplitude, for *L/D* = 20 and *e/D* = 1, are depicted in Fig. 10a, b respectively. The values of the parameter D_p has been found to vary from 0.8 to 0.94 in the ranges of $1 \le N \le 1,000$ and $0.1 \le A \le 0.5$. The degradation factor is observed to decrease fairly linearly with $\log_{10}N$; the slopes of these straight lines do not vary significantly for different values of the

amplitude. With respect to the amplitude *A*, the parameter D_p is found to decrease (Fig. 10b), the average slopes being quite small (<5%). In other words, the alteration in amplitude produces limited effect on the degradation factor. It has also been observed that up to $A = 0.2$, the relationship is fairly linear and thereafter parabolic with increasing slope. Although the soil degradation factor is independent of the amplitude of cyclic load applied on the pile head, the latter affects the depth of soil yield thereby indirectly influencing the value of cyclic axial pile capacity. At higher amplitude of $A > 0.2$, the depth of soil yield below the ground surface progressively increases which reduces the cyclic pile capacity.

4.2.2 Accumulated Pile Head Deflection

The accumulated pile head deflection, normalized as ρ_h/D, has been plotted against increasing number of cycles and amplitude (Fig. 11a, b) for *L/D* = 20 and *e/D* = 1. The parameter ρ_h/D has been observed to increase quite sharply for the initial range of $1 < \underline{N} \le 50$ and stabilizes abruptly thereafter. The stabilized values of ρ_h/D are found to vary from 5 to 43%. It has also been noted that under identical conditions, the accumulated pile head deflection for free headed pile is slightly greater in comparison to the fixed head condition. With the increasing amplitude, on the other hand, the accumulated deflection is found to increase following parabolic pattern with increasing slopes.
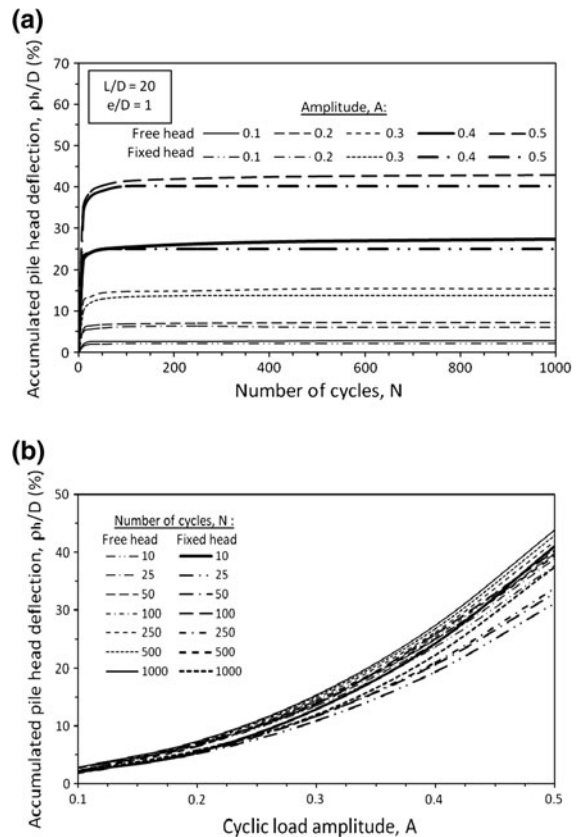
4.2.3 Bending Moment Profiles

The bending moment produced in the piles, normalized by $K_p\gamma'D^4$, are plotted against normalized depth *z/L* for the two pile head conditions (Fig. 12a, b). Analysis is carried out for three different values of *L/D*, viz., 10, 20 and 30. The *L/D* ratio has been observed to produce remarkable effect especially on the magnitude of maximum bending moment, although the effect of *N* is rather insignificant except increasing the magnitude slightly. The basic nature of the bending moment profiles are found to be in reasonably agreement with those found by other researchers (Matlock 1970; Basack 1999; Dyson 1999). The differences in the pattern for the two pile head conditions mainly arise out of the fixing moment developed due to head fixity.
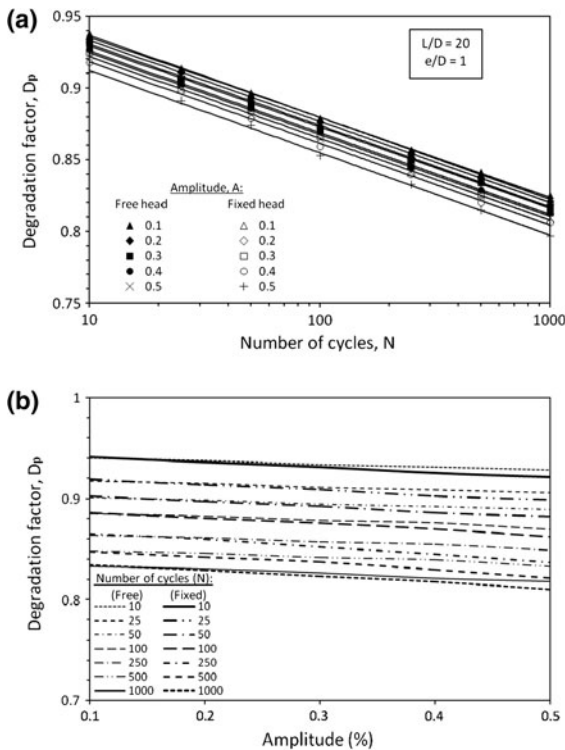
Fig. 10 Variation of D_p with: **a** N. **b** A

Fig. 11 Variation of cumulative pile head deflection with: **a** N. **b** A

For free headed pile, the bending moment is positive at the ground surface (=H·e) and increases with depth till a maximum value is attained and thereafter decreases non linearly with further increase of z/L; the bending moment at pile tip is zero (assumption iv in the Sect. 2.1 above). For L/D = 10, the maximum normalized bending moment is found to vary in the range of 22–25 for $1 \leq N \leq 1,000$, against the values of about 52–56 and 53–57 for the L/D ratios of 20 and 30 respectively. The values of normalized depth z/L for the occurrence of these maximum bending moments are respectively about 0.27, 0.2 and 0.12 for the L/D ratios of 10, 20 and 30. Slight negative bending moment in the order of −0.5 to −1.0 is noted near pile base for L/D ratios of 20 and 30.

In case of the fixed pile head condition, on the other hand, the bending moment is observed to be negative at the ground surface. With increase in z/L, the bending moment increases following a curvilinear pattern, passes through the point of contraflexure, attains a maximum positive value and thereafter decreases with depth to zero at the pile base. For $1 \leq N \leq 1,000$, the

magnitudes of normalized bending moment at ground surface and maximum positive bending moment are observed to vary in the range of about 12–13, 85–90 and 90–98 and 15–16, 34–37 and 38–42 for the L/D ratios of 10, 20 and 30 respectively. While the depth point of contraflexure varied between $0.08 < z/L < 0.14$, the values of z/L for occurrence of the maximum positive bending moment are 0.45, 0.3 and 0.2 for the L/D ratios of 10, 20 and 30 respectively.

4.2.4 Influence of K_{rs} and Design Recommendations

The parameter K_{rs} was observed to remarkably affect the cyclic pile response, although the influence of e/D was rather insignificant. Previously (see Sect. 4.3.2) it was found that the D_p decreases with $log_{10}N$ following a linear pattern, the slope of which does not vary notably with alteration of the amplitude. Also, D_p decreases with cyclic load amplitude fairly linearly. With these observations, the degradation function D_f,
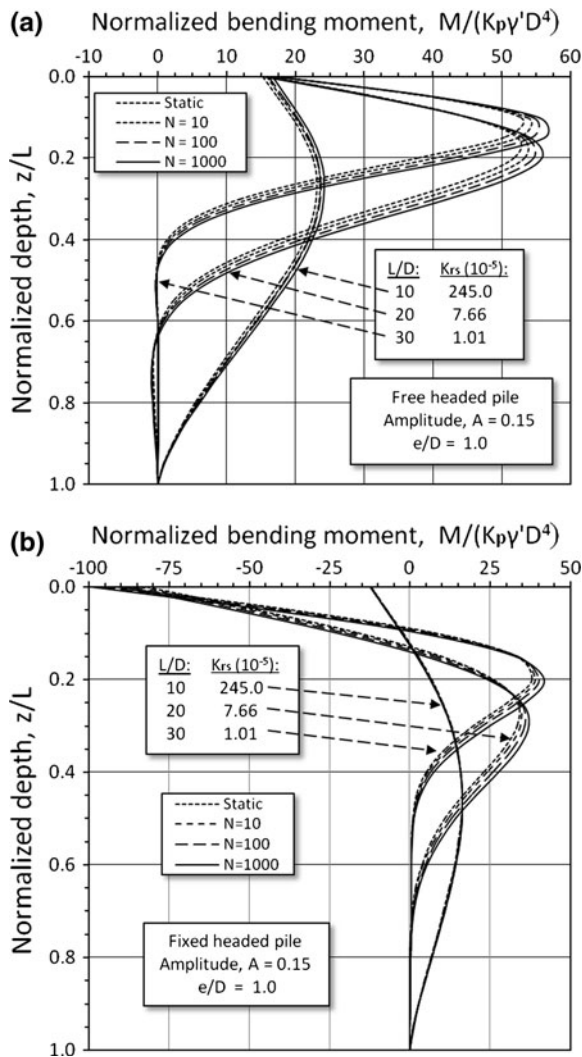
Fig. 12 Bending moment diagrams for: **a** free headed pile. **b** Fixed headed pile

a non-dimensional quantity defined in the Eq. 11 below, has been plotted against e/D for different values of K_{rs} (Fig. 13).

$$D_f = \frac{1 - D_p}{A \log_{10} N} \qquad (11)$$

Essentially such a set of curves is valid for the present case study, i.e., driven pile in dense sand subjected to symmetric two way lateral cyclic loading. Similar curves can also be plotted for other conditions of soil density, pile installation and cyclic loading pattern by using suitable values of the coefficients F_L, F_I and F_D from Long and Vanneste (1994). These sets

of curves can be utilized for design of pile in given sand subjected to cyclic lateral loading with desired number of cycles and amplitude.

With the increase of e/D, degradation function D_f was observed (Fig. 13) to decrease non-linearly with decreasing slope in the ranges of $0 \leq e/D \leq 2$ and $0 \leq e/D \leq 4$ for the free headed and the fixed headed piles respectively and thereafter assumes constant value.

5 Limitations of Analysis

While the boundary element analysis described above can predict the single pile response to lateral cyclic loading in sand to an acceptable accuracy, it has inherent limitations as follows:

(i)   Single pile response to lateral loading is affected by the application vertical load on the pile head (Anagnostopoulos and Georgiadis 1993). The model is unable to incorporate this aspect.

(ii) The model cannot be directly used to a layered soil, although by adopting certain engineering judgement (like using average soil parameters with more weighting being given to the upper layers), an approximate analysis can be performed.

(iii) In reality, the application of vertical load on the pile induces shear stress between the soil and the pile at the interface. Application of such shear stress may influence the magnitude of the yield stress p_{ui}, as used in the analysis (Poulos and Davis 1980). At the same time, the flexural equations for the pile should as well be modified introducing a beam-column analysis.

6 Conclusions

A boundary element analysis for predicting the single pile response to lateral cyclic loading in sand has been carried out based on elastic analysis and semi-empirical correlations for soil degradation. The comparison of the numerical results with the available laboratory model experimental and field test results justifies the validity of the proposed model.

The study indicates that the normalized lateral static capacity varies in the range of 20–130 for free

Fig. 13 Variation of D_f with e/D
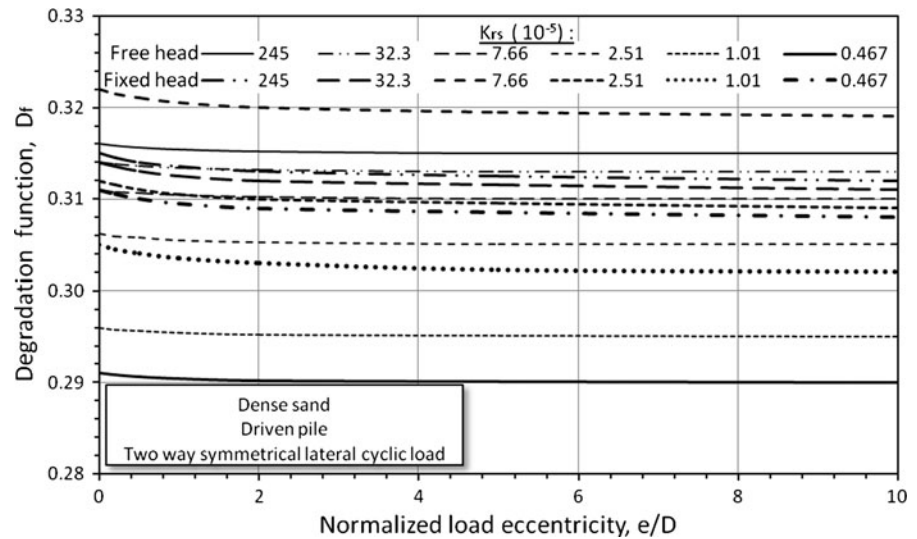
headed pile against 40–280 under fixed head condition. The capacity decreases quite sharply in a curvilinear manner with decreasing slope for $K_{rs} \leq 10^{-3}$ and stabilizes thereafter. Similar trend is observed when the lateral static pile is plotted against the normalized load eccentricity, the rate of decrease is quite sharp for $10 \leq L/D \leq 15$ and in the range of $0 \leq e/D \leq 4$. For identical parameters, the head fixity is observed to produce significant increase in the static lateral pile capacity. The capacity factor C_f is found to vary between 1.67 and 2.4. With increasing K_{rs}, C_f decreases quite sharply for intial values of $K_{rs} \leq 2.5 \times 10^{-4}$, attains a minimum value and thereafter increases linearly.

While the pile response under cyclic lateral loading is studied, the parameter D_p is found to vary in the range of 0.8–0.94 for $1 \leq N \leq 1,000$ and $0.1 \leq A \leq 0.5$. The degradation factor is observed to decrease fairly linearly with $\log_{10}N$. The increasing cyclic load amplitude produced only a slight reduction of the value of D_p. The relationship is observed to be fairly linear for $A \leq 0.2$, and parabolic with increasing slope thereafter. The accumulated pile head deflection produced under lateral cyclic loading is observed to increase quite sharply for the initial range of $N \leq 50$ and thereafter stabilizes abruptly. These stabilized values are found to vary from 5 to 43%. With the increasing amplitude, the accumulated deflection is found to increase following parabolic pattern with increasing slope.

The non linear nature of the bending moment profiles are found to be similar to those found by the other researchers. The L/D ratio produced remarkable effect on the magnitude of maximum bending moment, although the effect of N is insignificant. For free headed pile, the positive bending moment increases with depth till a maximum value is attained, thereafter decreases non-linearly to zero at pile base. A slight negative bending moment is noted near the pile base for higher L/D ratios. The maximum bending moment is found to increase both in its magnitude and depth of occurrence with increase in L/D ratio. In case of fixed headed pile, the bending moment increases with depth starting from a negative value at ground surface, passes through the point of contraflexure, attains the maximum positive value, and thereafter decreases to zero at the pile base. The variation in L/D ratio is observed to significantly influence both on the magnitudes of bending moment and depths of contraflexure and maximum positive value.

For specified cyclic loading parameters, the variation of K_{rs} influences the lateral cyclic pile response quite remarkably. With the increase of e/D, degradation function D_f decreases non-linearly with decreasing slope in the range of $0 \leq e/D \leq 2$ and $0 \leq e/D \leq 4$ for the free headed and the fixed headed piles respectively and thereafter assumes constant value. The set of curves for D_f versus e/D for various K_{rs} and pile head conditions can be utilized for design of pile subjected to lateral cyclic loading.

The main significance of the research described in this paper is its usefulness to the practicing geotechnical engineers for the design of pile in sand subjected

to lateral cyclic loading. As portrayed in Fig. 13, where the curves relating D_f versus e/D for different values of K_{rs} are presented in the case of a driven pile in dense sand subjected to a two way symmetrical lateral cyclic loading, similar sets of design curves can as well be plotted (using the present boundary element model) for the other conditions of pile installation, soil density and cyclic loading pattern, as the practical situation would demand. These curves can be utilized to reasonably estimate the degradation in pile capacity, and hence the factor of safety against failure, for the design values of relative pile-soil stiffness, load eccentricity and cyclic load amplitude at the desired number of cycles.

7 Acknowledgement

References

Allotey N, El Naggar MH (2008) A numerical study into lateral cyclic nonlinear soil-pile response. Can Geotech J 45:1268–1281

Anagnostopoulos C, Georgiadis M (1993) Interaction of axial and lateral pile responses. J Geotech Eng Div ASCE 119(4):793–798

Ashour M, Norris GM (1999) Liquefaction and undrained response evaluation of sands from drained formulation. J Geotech Geoenviron Eng ASCE 125(8):649–658

Basack S (1999) Behaviour of pile under lateral cyclic loading in marine clay. PhD thesis, Jadavpur University, Calcutta, India

Basack S (2008a) A boundary element analysis of soil pile interaction under lateral cyclic loading in soft cohesive soil. Asian J Civil Eng (Building and Housing) 9(4):377–388

Basack S (2008b) Degradation of soil pile interactive performance under lateral cyclic loading. Final Technical Report University Grants Commission UGCAM/SB/107/FINAL, Bengal Engineering and Science University, Howrah, India

Basack S (2010a) Response of pile group subjected to lateral cyclic load in soft clay. Latin Am J Solids Struct 7(2):91–103

Basack S (2010b) A boundary element analysis to study the influence of k_{rc} and e/d on the performance of cyclically loaded single pile in clay. Latin Am J Solids Struct 7(3):265–284

Bea RG, Aurora RP (1982) Design of pipelines in mudslide areas. In: Proceedings of 14th annual OTC Houston, vol 1, no OTC 4411, pp 401–414

Broms BB (1964a) Lateral resistance of pile in cohesive soils. J Soil Mech Found Div ASCE 90(SM2):27–63

Broms BB (1964b) Lateral resistance of pile in cohesionless soils. J Soil Mech Found Div ASCE 90(SM3):123–156

Douglas DJ, Davis EH (1964) Movement of buried footing due to moment and horizontal load and movement of anchor plates. Geotechnique 14:115–132

Dyson GJ (1999) Lateral loading of piles in calcareous sediments. PhD thesis, Department of Civil Research Engineering, University of Western Australia, Perth

Gudehus G, Hettler A (1981) Cyclic and monotonous model tests in sand. In: Proceedings of international conference of soil mechanics and foundation engineering, Stockholm, vol 2, pp 211–214

Kulhawy FW, Mayne PW (1990) Manual on estimating soil properties for foundation design. Final report of research project 1493-6, Geotechnical Engineering Group, Cornell University, New York, USA

Long JH, Vanneste G (1994) Effects of cyclic lateral loads on piles in sand. J Geotech Engrg Div ASCE 120(1):225–244

Matlock H (1970) Correlations for design of laterally loaded piles in soft clay. In: Proceedings of 2nd annual OTC, Houston, vol 1, pp 577–594

Matlock H, Foo SHC, Bryant LM (1978) Simulation of lateral pile behavious under earthquake motion. In: Procedings of conference earthquake engineering and soil dynamics ASCE, vol 2, pp 600–619

Mindlin RD (1936) Force at a point in the interior of a semi-infinite solid. Physics 7:195–202

Narasimha Rao S, Prasad YVSN (1993) Uplift behavior of pile anchors subjected to lateral cyclic loading. J Geotech Engrg Div ASCE 119(4):786–790

Poulos HG (1971) Behavior of laterally loaded pile: I—single piles. J Soil Mech Found Div ASCE 97(SM-5):711–731

Poulos HG (1981) Cyclic axial response of single pile. J Geotech Eng Div ASCE 107(GT1):355–375

Poulos HG (1982) Single pile response to cyclic lateral load. J Geotech Eng Div ASCE 108(GT3):355–375

Poulos HG (1988) Marine geotechnics. Unwin Hyman, London

Poulos HG, Davis EH (1980) Pile foundation analysis and design. Wiley, New York

Purkayastha RD, Dey S (1991) Behavior of cyclically loaded model piles in soft clay. In: Proceedings of 2nd international conference on recent advances in geotechnical earthquake engineering soil dynamics, University of Missouri-Rolla, USA, vol 1, pp 212–215

Reese LC (1977) Laterally loaded piles: program documentation. J Geotech Eng Div ASCE 103(GT4):287–305

Robertson PK, Campanella RG (1983) Interpenetration of cone penetration tests. Can Geotech J 20(4):718–733

Taylor AJ (2006) Full-scale lateral load test of a 1.2 m diameter drilled shaft in sand. M. Sc. thesis, Department of Civil and Environmental Engineering, Brigham Young University, Provo, UT, USA

Terzaghi K (1955) Evaluation of coefficients of sub-grade reactions. Geotechnique 5:297–315